Supplementary Information

Phosphorus/Nitrogen Co-Doped and Bimetallic MOFs-Derived Cathode for All-Solid-State Rechargeable Zinc-Air Battery

Xing Yang,[a1] Xianghua Wu,[a1] Zeping Guo,[a] Qingyu Li,[be] Hongqiang Wang,[*be] Chujun Ke,[a] Wei Zeng,[a] Xiafei Qiu,[a] Yun He,[*ae] Xiaoguang Liang,[*abd] and Yoonseob Kim[c]

[a]Department of Physics, Guangxi Normal University, Guilin, China

[b]Guangxi Key Laboratory of Low Carbon Energy Materials, Guangxi Normal University, Guilin, China

[c]Department of Chemical and Biological Engineering, Hong Kong University of Science and Technology, Clear Water Bay, Kowloon, Hong Kong SAR, China

[d]Guangxi Key Laboratory of Nuclear Physics and Technology, Guangxi Normal University, Guilin, China

[e]State Key Laboratory for Chemistry and Molecular Engineering of Medicinal Resources, Guangxi Normal University, Guilin, China

*Corresponding authors.

Email: lxg8521@mailbox.gxnu.edu.cn (X.G. Liang), hy@gxnu.edu.cn (Y. He), whq74@gxnu.edu.cn (H.Q. Wang)

[1]These authors contributed equally to this work.

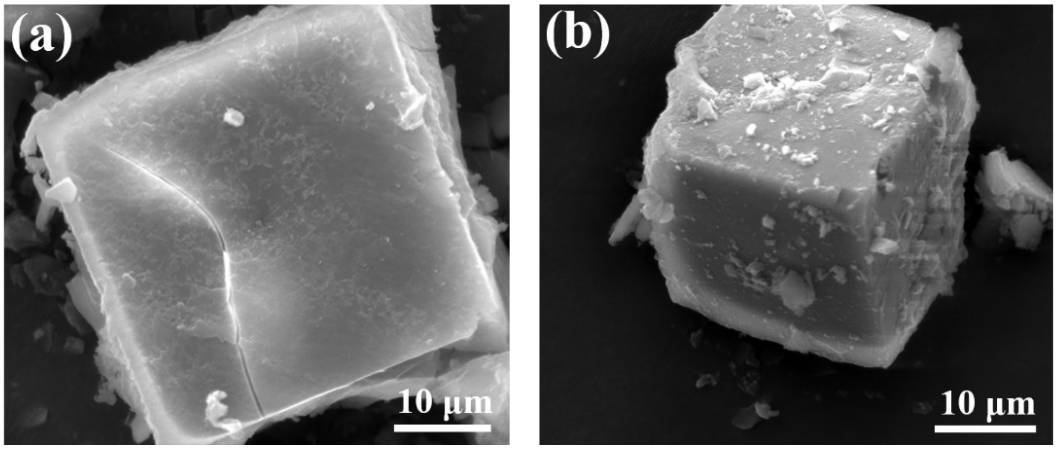

Fig. S1. SEM images of FeNi-MOFs. (a) Top view and (b) Side view.

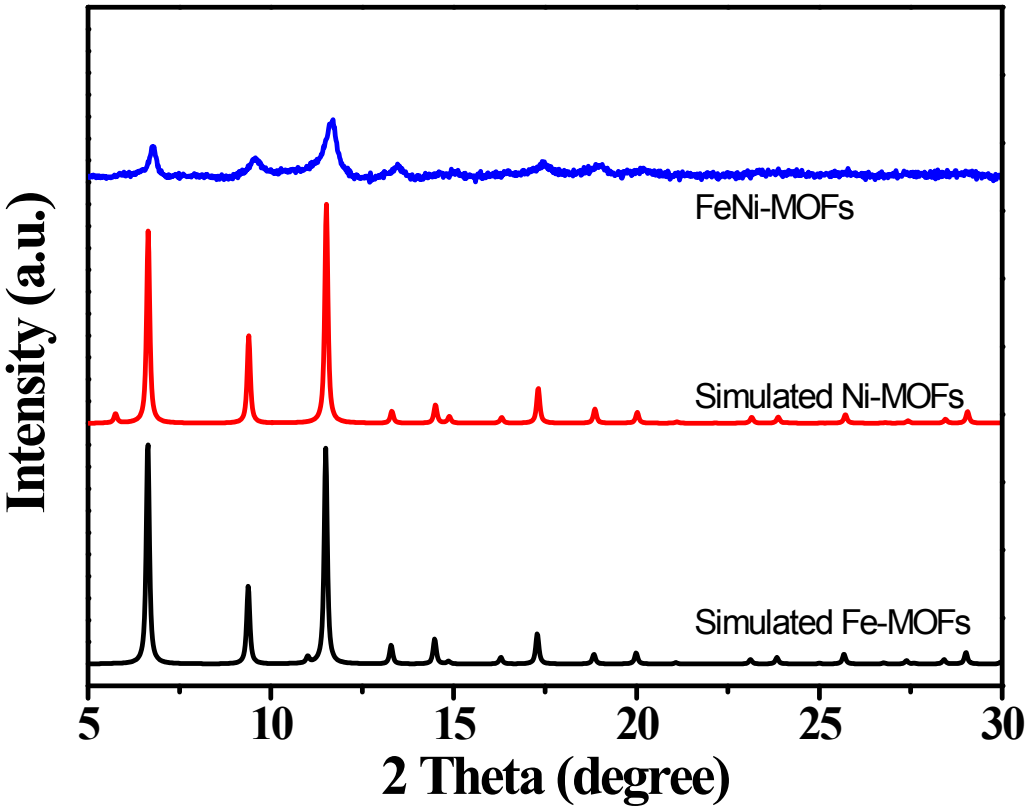

Fig. S2. The XRD pattern of FeNi-MOFs.

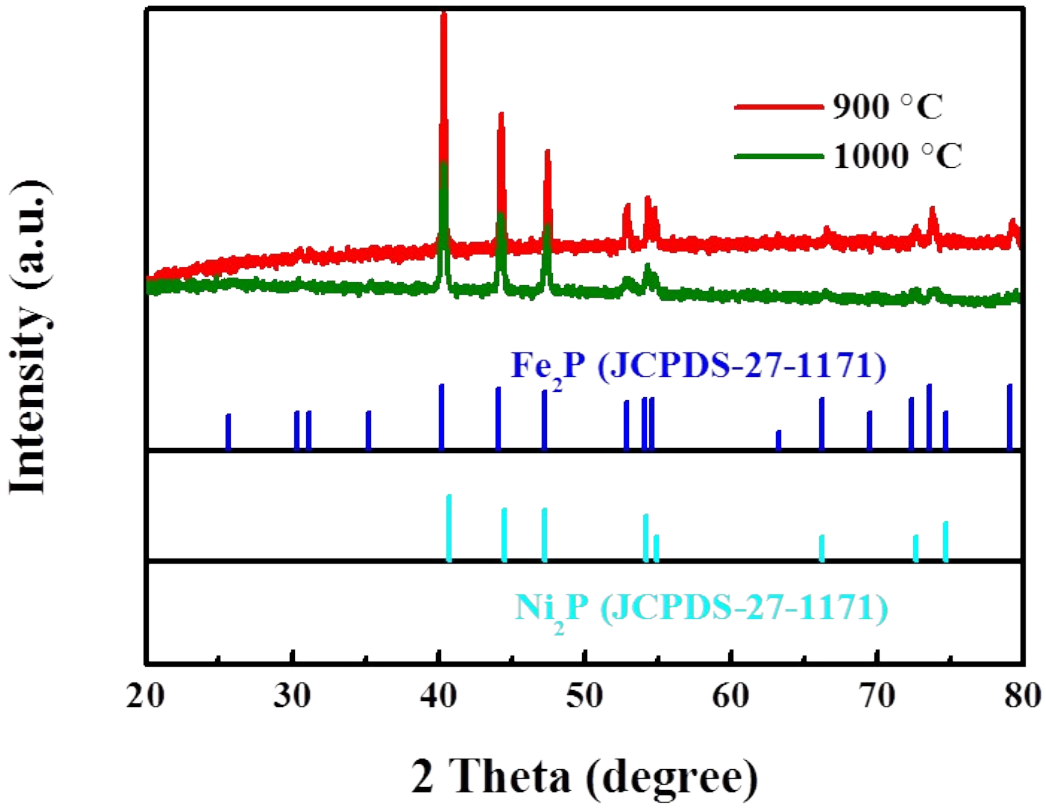

Fig. S3. The XRD patterns of P-FeNi/NC@G synthesized at different temperature.

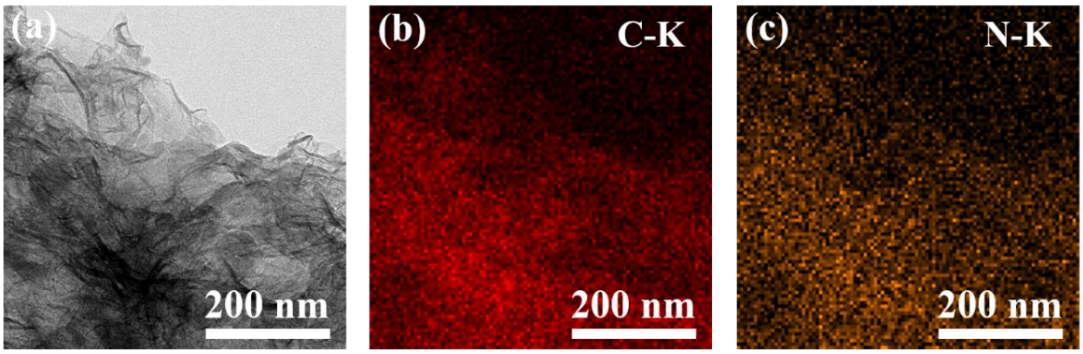

Fig. S4. TEM image and the corresponding EDS elemental mapping images of C, N elements.

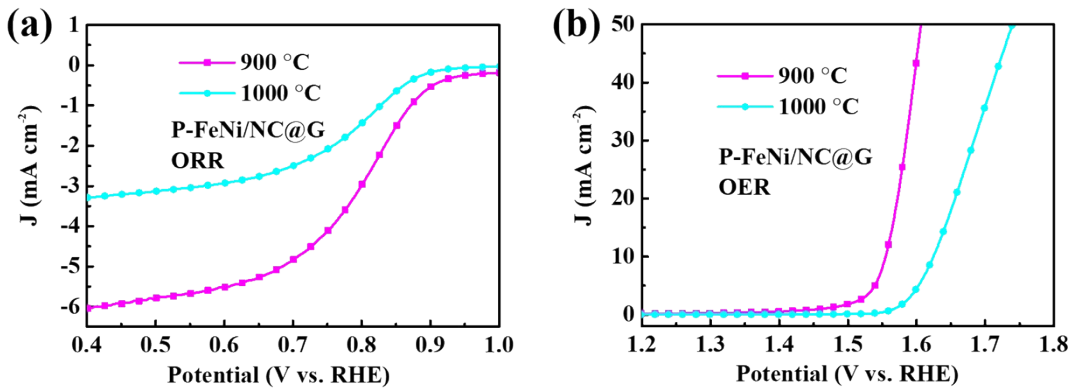

Fig. S5. (a) ORR and (b) OER polarization curves tested in O_2-saturated 0.1 M KOH at 1600 rpm. The P-FeNi/NC@G catalysts are synthesized at different pyrolysis temperature of 900 ℃ and 1000 ℃ in argon atmosphere.

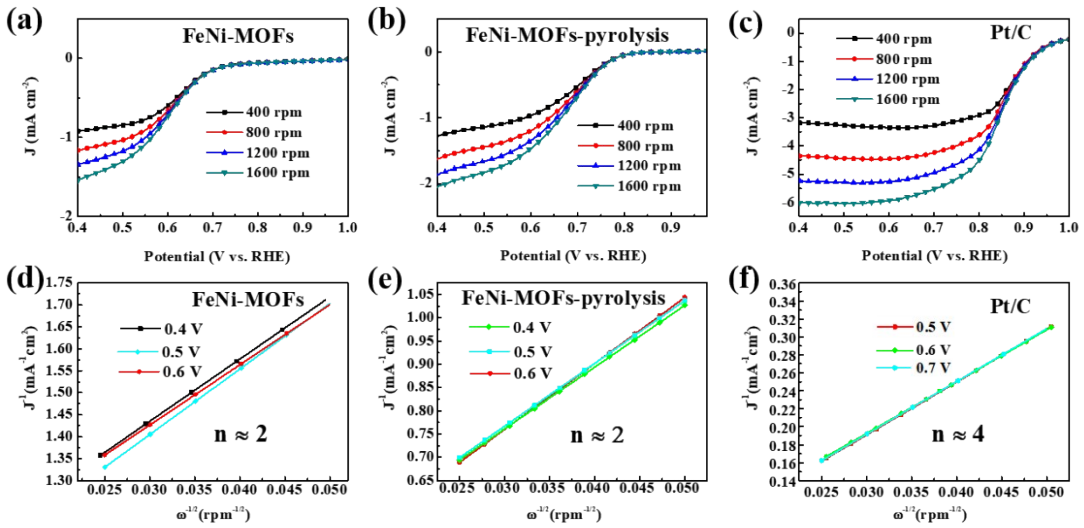

Fig. S6. ORR polarization curves of (a) FeNi-MOFs, (b) FeNi-MOFs-pyrolysis and (c) commercial Pt/C tested in O_2-saturated 0.1 M KOH at different Rotation speeds. (d)-(f) The corresponding K-L plots at different potentials and the calculated electron transfer number per oxygen molecule (n).

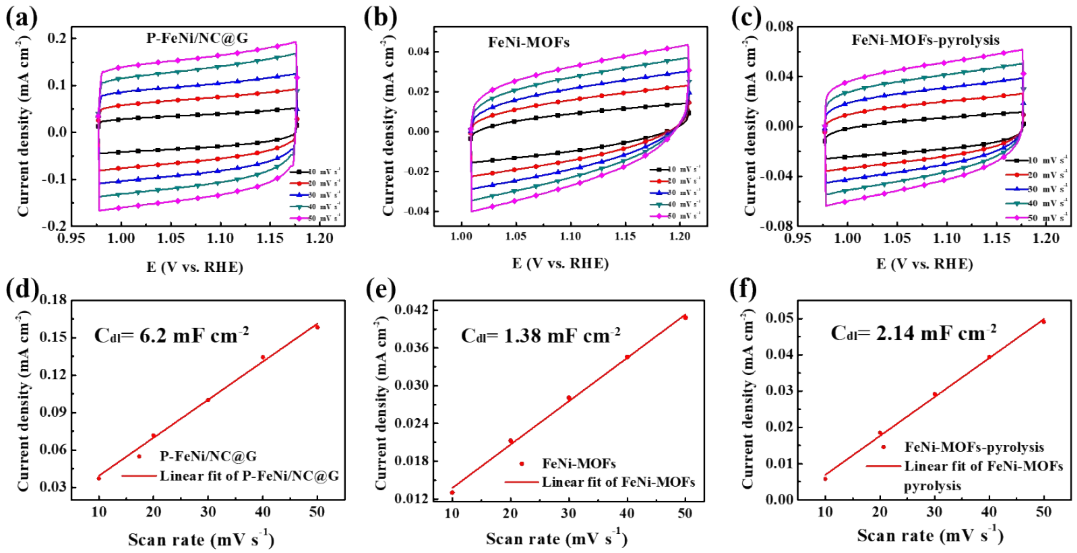

Fig. S7. CV curves in the range of 0-0.2 V at scan rates from 10 to 50 mV s^{-1} and corresponding current density-scan rates curves. (a) and (d) for P-FeNi/NC@G, (b) and (e) for FeNi-MOFs, (c) and (f) for FeNi-MOFs-pyrolysis.

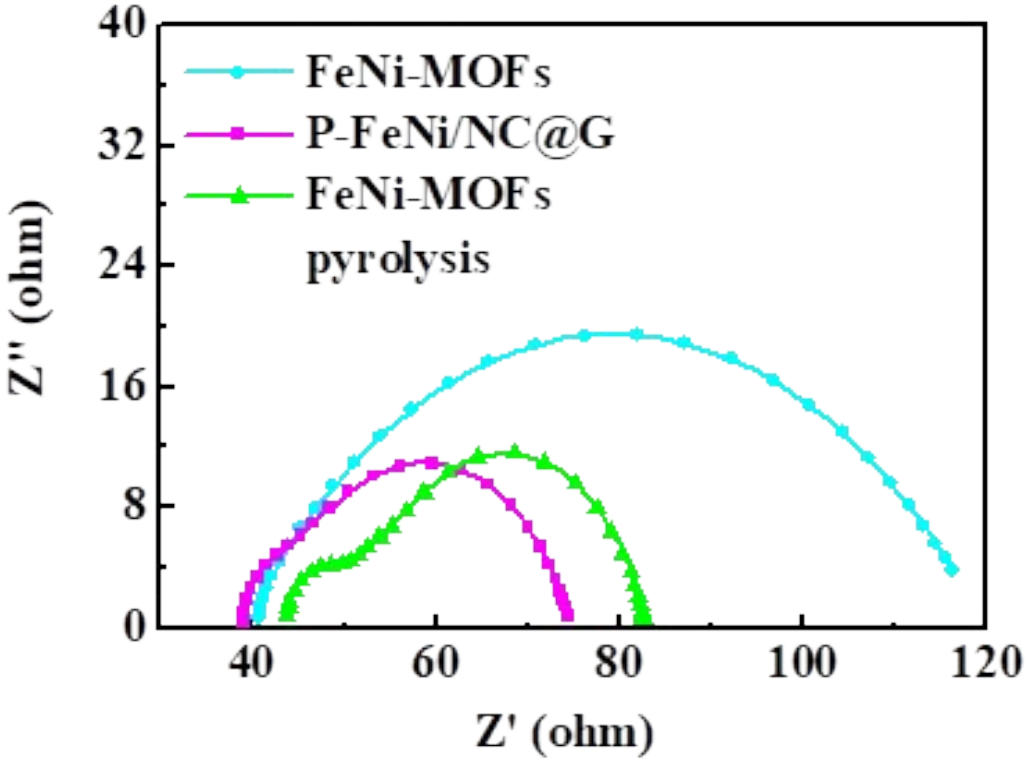

Fig. S8. Nyquist plots of FeNi-MOFs, FeNi-MOFs-pyrolysis, and P-FeNi/C@G catalysts.

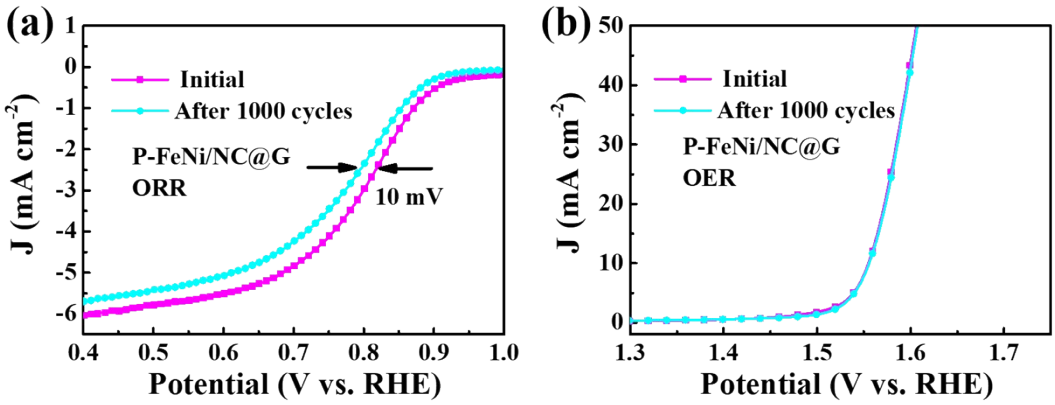

Fig. S9. The (a) ORR and (b) OER LSV curves of P-FeNi/NC@G catalyst recorded before and after 1000 CV cycles.

Table S1. The ΔE value of different catalysts.[#]

Catalysts	$E_{1/2}$ (V)	$E_{j=10}$ (V)	ΔE (V)
FeNi-MOFs	0.64	1.65	1.01
FeNi-MOFs-pyrolysis	0.71	1.60	0.89
Pt/C	0.84	1.86	1.02
RuO_2	0.60	1.56	0.96

[#]$E_{1/2}$ is the half over-potential of ORR, $E_{j=10}$ is the potential of OER at a current density of 10 mA cm^{-2}, ΔE is the potential difference between $E_{j=10}$ and $E_{1/2}$.

Table S2. List of properties of recently reported all-solid-state ZABs based on other cathodic catalysts.

Catalysts	$E_{1/2}$ (V)	$E_{j=10}$ (V)	ΔE (V)	Power density (mW cm^{-2})	Reference
P-FeNi/NC@G	0.81	1.54	0.73	159	**This work**
Co_2P@CNF	0.803	1.691	0.88	121	S1
CoNi-MOF/RGO	0.718	1.548	0.83	97	S2
Hybrid nanosheets	0.79	1.72	0.93	—	S3
FeN_x-PNC	0.86	1.635	0.775	118	S4
Fe-CoN_4@NC	0.83	1.62	0.79	105	S5
FeNi@NCNTs/CC	0.77	1.48 (1M KOH)	0.71	—	S6
Co_3O_{4-x} HoNPs@HPNCS-60	0.83	1.57	0.74	94.1	S7
NiCo/PFC	0.79	1.63	0.84	—	S8
N-GCNT/$FeCo_3$	0.92	1.73	0.81	97.6	S9
EA-Ni-900	0.78	1.55	0.77	65	S10
CC-AC	0.72	1.59	0.87	52.3	S11
FeNi-LDH@3DG/CNTS	0.71	1.61	0.9	—	S12
Fe-Ni_2P@N, P-CNS	0.75	1.62	0.87	—	S13
N-$CoSe_2$/3D Ti_3C_2TX	0.79	1.54	0.75	142	S14
FeNi-NC	0.83	1.61	0.78	80.8	S15
NiFe/N-CNT	0.75	1.52	0.77	105.4	S16

Reference

[S1] J. Gao, J. Wang, L. Zhou, X. Cai, D. Zhan, M. Hou, L. Lai, Co_2P@N,P-codoped carbon nanofiber as a free-standing air electrode for Zn-air batteries: synergy effects of CoNx satellite shells, ACS Appl. Mater. Interfaces 11 (2019) 10364–10372.

[S2] X. Zheng, Y. Cao, D. Liu, M. Cai, J. Ding, X. Liu, J. Wang, W. Hu, C. Zhong, Bimetallic metal-organic-framework/reduced graphene oxide composites as bifunctional electrocatalysts for rechargeable Zn-air batteries, ACS Appl. Mater. Interfaces 11 (2019) 15662–15669.

[S3] Y. Li, C. Zhong, J. Liu, X. Zeng, S. Qu, X. Han, Y. Deng, W. Hu, J. Lu, Atomically thin mesoporous Co_3O_4 layers strongly coupled with N-rGO nanosheets as high-performance bifunctional catalysts for 1D knittable zinc-air batteries, Adv Mater. 30 (2018) 1703657.

[S4] L. Ma, S. Chen, Z. Pei, Y. Huang, G. Liang, F. Mo, Q. Yang, J. Su, Y. Gao, J.A. Zapien, C. Zhi, Single-site active iron-based bifunctional oxygen catalyst for a compressible and rechargeable zinc-air battery, ACS Nano 12 (2018) 1949–1958.

[S5] Q. Jin, B. Ren, J. Chen, H. Cui, C. Wang, A facile method to conduct 3D self-supporting Co-FeCo/N-Doped graphene-like carbon bifunctional electrocatalysts for flexible solid-state zinc air battery, Appl. Catal., B 256 (2019) 117887.

[S6] X. Zhao, S.C. Abbas, Y. Huang, J. Lv, M. Wu, Y. Wang, Robust and highly active FeNi@NCNT nanowire arrays as integrated air electrode for flexible solid-state rechargeable Zn-air batteries, Adv. Mater. Interfaces 5 (2018) 1701448.

[S7] D. Ji, L. Fan, L. Tao, Y. Sun, M. Li, G. Yang, T.Q. Tran, S. Ramakrishna, S. Guo, The Kirkendall Effect for engineering oxygen vacancy of hollow Co_3O_4 nanoparticles toward high-performance portable zinc-air batteries, Angew. Chem., Int. Ed. 58 (2019) 13840–13844.

[S8] G. Fu, Y. Chen, Z. Cui, Y. Li, W. Zhou, S. Xin, Y. Tang, J.B. Goodenough, Novel hydrogel-derived bifunctional oxygen electrocatalyst for rechargeable air cathodes, Nano Lett 16 (2016) 6516–6522.

[S9] C. Su, H. Cheng, W. Li, Z.Liu, N. Li, Z. Hou, F. Q. Bai, H. Zhang, T. Ma, Atomic modulation of FeCo-nitrogen-carbon bifunctional oxygen electrodes for rechargeable and flexible all-solid-state zinc-air battery, Adv. Energy Mater. 7 (2017) 1602420.

[S10] J. Zhao, R. Qin, R. Liu, Urea-bridging synthesis of nitrogen-doped carbon tube supported single metallic atoms as bifunctional oxygen electrocatalyst for zinc-air battery, Appl. Catal., B 256 (2019) 117778.

[S11] K. Kordek, L. Jiang, K. Fan, Z. Zhu, L. Xu, M. Al-Mamun, Y. Dou, S. Chen, P. Liu, H. Yin, P. Rutkowski, H. Zhao, Two-step activated carbon cloth with oxygen-rich functional groups as a high-performance additive-free air electrode for flexible zinc-air batteries, Adv. Energy Mater. 9 (2019) 1802936.

[S12] Y. Li, M. Zhao, Y. Zhao, L. Song, Z. Zhang, FeNi layered double-hydroxide nanosheets on a 3D carbon network as an efficient electrocatalyst for the oxygen evolution reaction, Part. Part. Syst. Charact. 33 (2016) 158–166.

[S13] Y. Xiao, S. Deng, M. Li, Q. Zhou, L. Xu, H. Zhang, D. Sun, Y. Tang, Immobilization of Fe-doped Ni_2P particles within biomass agarose-derived porous N,P-carbon nanosheets for efficient bifunctional oxygen electrocatalysis, Front. Chem. 7 (2019) 523.

[S14] Z. Zeng, G. Fu, H.B. Yang, Y. Yan, J. Chen, Z. Yu, J. Gao, L.Y. Gan, B. Liu, P. Chen, Bifunctional N-$CoSe_2$/3D-MXene as highly efficient and durable cathode for rechargeable Zn–air battery, ACS Materials Lett. 1 (2019) 432–439.

[S15] L. Yang, X. Zeng, D. Wang, D. Cao, Biomass-derived FeNi alloy and nitrogen-codoped porous carbons as highly efficient oxygen reduction and evolution bifunctional electrocatalysts for rechargeable Zn-air battery, Energy Storage Mater 12 (2018) 277–283.

[S16] H. Lei, Z. Wang, F. Yang, X. Huang, J. Liu, Y. Liang, J. Xie, M.S. Javed, X. Lu, S. Tan, W. Mai, NiFe nanoparticles embedded N-doped carbon nanotubes as high-efficient electrocatalysts for wearable solid-state Zn-air batteries, Nano Energy 68 (2020) 104293.